RC frame structures retrofitted by FRP-wrapping: A model for columns under axial loading and cyclic bending

RC FRAME STRUCTURES RETROFITTED BY FRP-WRAPPING: A MODEL FOR COLUMNS UNDER AXIAL LOADING AND CYCLIC BENDING

Barbara Ferracuti[1], Marco Savoia[2], and Maria Zucconi[3]

[1,3]*Niccolò Cusano University, Roma, Italy*

[2]*DICAM - Structural Engineering, University of Bologna, Bologna, Italy*

ABSTRACT

In order to mitigate the seismic risk of existing RC frame structures not designed with seismic criteria, a widespread strengthening strategy is based on increasing strength and ductility of RC columns by means of Fiber Reinforced Polymer wrapping. The existing models for RC cross-sections wrapped by FRP sheets were developed principally considering pure axial loads with uniform confinement pressure. In seismic areas, RC columns are instead usually subjected to axial load and cyclic bending. In the present work, in order to consider the effective loading conditions, an iterative cyclic model for square RC cross-sections wrapped by composite FRP sheets subjected to axial force and cyclic bending is proposed. The model considers the strain gradient-effect over the cross-section due to the bending loads that change significantly the confinement level of RC cross-section. Moreover, the model has been validated by comparing the numerical outcomes with various cyclic experimental results. The model has been also implemented in an open-source software with distributed plasticity finite elements in order to perform pushover analyses of an existing RC frame structure with different retrofitting strategies to improve the ductility of the columns for lateral forces.

KeyWords: FRP – wrapping; RC column; confinement; cyclic constitutive law; axial force and cyclic bending; distributed plasticity; pushover analysis.

---

[1] Associate Professor – Via Don Carlo Gnocchi 3, 00166 Roma, Italy, barbara.ferracuti@unicusano.it

[2] Full Professor – Viale Risorgimento 2, 40136 Bologna, Italy, marco.savoia@unibo.it

[3] Assistant Professor – Via Don Carlo Gnocchi 3, 00166 Roma, Italy, maria.zucconi@unicusano.it, corresponding author.

1 INTRODUCTION

The seismic vulnerability of Reinforced Concrete -RC- frame structures not designed with earthquake engineering criteria leads to high economic losses and a significant number of casualties, as observed in the aftermath of severe earthquakes [1–4] or in numerical Loss Analysis simulations [5–7]. In order to improve the seismic response of RC frames, an intervention able to increase the deformation capacity in the nonlinear range with a high value of energy dissipation is desirable. Such behavior can be obtained by means of FRP (Fiber Reinforced Polymer) wrapping. This kind of intervention was proposed more than 30 years ago to increase the strength of RC columns subject to high axial loadings. Only later, FRP-wrapping has been considered a very effective strengthening technique for RC structures under seismic actions [8]. In fact, several experimental tests showed that strengthening by FRP - wrapping increases significantly the ductility of columns under cyclic bending moment due to the earthquake action [9–16]. The experimental studies on FRP-confined columns with square or rectangular cross-section presented in the literature are limited in number. Among them, Sheikh and Yau [9], early 2002, realized an extensive campaign on circular columns wrapped with FRP subjected to axial load and reversed cyclic lateral loads. Memon and Sheikh [11] performed cyclic tests on square RC columns retrofitted with glass FRP sheets. One interesting experimental campaign was conducted by Realfonzo and Napoli [13], i.e., full-scale tests performed on rectangular RC columns externally confined by FRP wrapping or FRP wraps and longitudinal steel profiles. The study was a part of a broader experimental campaign on square RC columns. Moreover, Ghatte et al. [14] tested five full-scale rectangular RC columns under constant axial load and cyclic lateral loads along their strong or weak planes before and after retrofitting with FRP wrapping.

From the numerical point of view, several constitutive laws can be found in the literature for FRP-wrapped columns subject to pure axial compression. In particular, most of the models [17–19] consider a constant lateral pressure due to FRP wrapping independently to the loading level, according to models adopted for confinement by steel stirrups (design-oriented models). Nevertheless, confinement action of FRP sheets acts differently. Considering RC circular cross-sections, the effect of FRP sheets is a passive confinement activated by transversal dilatation due to longitudinal deformation, which increases with concrete dilatation because of the elastic behavior of the composite. Consequently, the

confinement pressure of concrete wrapped by FRP is always variable depending on the concrete axial strain.

The design-oriented models proposed in the literature consider the FRP confinement effect introducing the strong assumption of constant confinement pressure, depending on the ultimate strain in FRP - wrapping [20–23]. This simplified approach can predict well only the ultimate load for circular cross-sections under axial force because the whole section is subject to a uniform confinement pressure over the cross-section, whose maximum value can be defined as a function of a percentage of FRP ultimate strain.

Advanced iterative models account for the interaction between the concrete and the confining material through explicit equilibrium and radial displacement compatibility considerations, see for instance Mirmiran and Shahawy [24], Spoelstra and Monti [25], Fam and Rizkalla [26], Binici [27], Teng et al. [28], and Lim and Ozbakkaloglu [29] for analysis-oriented models, where the actual confinement stress due to the linear elastic behavior of FRP materials depends on the actual longitudinal stress level.

More recently, in order to represent the effective loading condition of columns of buildings in seismic areas, the research was focused on the extension of confinement concrete models to the case of axial loading and bending. The available models can be divided into two main typologies as far as the evaluation of the confinement effect of FRP is concerned, the first group is based on constant confinement pressure (designed oriented models) [30–32] and the second group of models considers a variable confinement pressure (analysis oriented models) [33].

Lam and Teng's model [20] for confined concrete, based on constant lateral pressure depending on FRP mechanical (strength, elastic modulus) and geometrical properties only, was adopted and extended to the case of eccentric loading considering a constant confinement pressure over the compression region of the cross-section by various researches [e.g. 14,31]. The assumption of confinement constant over the entire cross-section and for all the axial loading levels can lead to quite inaccurate results, because the confinement strictly depends on the level of longitudinal deformation and the strain gradient over the cross-section makes confinement pressure variable. The confinement pressure exerted on the concrete is in fact not uniform over the cross-section, with longitudinal strain varying from zero at the neutral axis to a maximum value at the extreme fibers of concrete. Consequently, the stress-strain response of columns subjected to eccentric loads is very different from columns subjected to centered loads. Among the most recent works, Teng et al. [31] proposed a numerical model to simulate the behavior of circular RC columns with

FRP jacketing, subjected to axial compression and lateral cyclic loads. The proposed cyclic model for confined concrete in compression considers a constant confinement lateral stress as a function of FRP mechanical and geometrical properties, according to Lam and Teng model [20]. It is worth noting that the model adopts the same constitutive law for all the confined concrete fibers, independently of the gradient of the strain diagram over the RC cross-section and of the load level. Another recent model on FRP-jacketed RC circular columns was proposed by Ismail et al. [32]. The adopted confined concrete law is based on the design-oriented model proposed by Fahmy and Wu [19], considering both axial and bending loadings. In particular, the research was focused on the prediction of ultimate displacement, adopting different design-oriented models for confined concrete. It is worth noting that the prediction of deformation capacity of columns is an important parameter to assess the effectiveness of the strengthening technique. Ghatte et al. [14] adopted different design-oriented models [18,20,22,23] to perform a sectional analysis and to evaluate the ultimate displacements. The comparison with experimental results underlines that most of the models provide conservative values for deformation capacity.

With reference to circular cross-sections, Binici and Mosalam [33] proposed to evaluate the effective confining stress distribution as a function of the maximum confinement pressure at the extreme compression fiber, by solving a differential equation based on a bond-slip model with the assumption of linear elastic behavior for both FRP and FRP - concrete bond-slip relationship. This equation assures the equilibrium of an infinitesimal concrete – FRP sheet element subjected to variable tension in the FRP-fiber (circumferential) direction admitting slip between FRP and concrete.

In the present paper, an iterative model for RC cross-sections with FRP – wrapping under axial compression and cyclic loading is proposed. Variability of confinement pressure over the cross-section is taken into account by determining the effective gradient strain profile over the concrete cross-section through an iterative procedure based on both equilibrium and compatibility equations. The actual confinement pressure over the depth of the cross-section has been computed by applying the analysis oriented model, Spoelstra and Monti's iterative model [25], considering the actual longitudinal strain profile due to compression and bending. Therefore, at each loading step, each fiber is characterized by a different concrete constitutive law, with confinement stress defined as a function of the specific longitudinal strain.

In order to account for the shape effect for squared FRP-wrapped columns, the cross-section is subdivided into sub-regions corresponding to unconfined and confined concrete by FRP

wrapping. Moreover, with the aim of describing the cyclic response of RC columns, ad hoc unloading branches are defined and the pinching effect of moment-curvature diagram under cyclic loading is accurately reproduced. Then, the assessment of the reliability of the proposed model is performed by comparing numerical results with some literature experimental findings [9,11,34], for circular/square cross-sections unwrapped and wrapped by means of FRP jackets.

Finally, the cyclic constitutive laws proposed in this study were implemented in OpenSees distributed plasticity finite elements in order to perform pushover analyses of a pre-code RC frame structure, characterized by a soft-floor mechanism, adopting different retrofitting strategies. Different proposals for the definition of the failure condition, i.e., the ultimate chord rotation criterion or the attainment of the ultimate strain for FRP confinement are adopted and the results are compared.

2 FRP-WRAPPED RC COLUMN UNDER COMPRESSION AND BENDING: THE PROPOSED CYCLIC MODEL

The proposed cyclic model for RC cross-section wrapped by FRP and subjected to axial loading and cyclic bending is based on a cross-section analysis accounting for the dependence of the lateral confinement stress on the longitudinal strain of concrete. The strain gradient-effect due to the bending loads is taken into account. For the cyclic behavior, the unloading curve from the compression state, the behavior of concrete under tension and, finally, the reloading curve from tension to compression are also accurately defined.

An iterative technique is adopted at each loading step, the iterative procedure is performed for each fiber of confined concrete, taking into account the variable confinement pressure over the cross-section, depending on the nonuniform axial strain distribution in concrete. In this manner, a different confinement pressure exerted by FRP sheet, f_l, is considered in each fiber as a function of the axial strain. The following assumptions are considered:

a) plain profile of longitudinal strain over the column cross-section;
b) perfect bonding between FRP-concrete. This hypothesis is valid for loading close to the column failure load;
c) cross-section modeled by dividing it into two regions for confined and unconfined concrete, identified by parabola arches according to Mirmiran et al. [35]. Then, the concrete cross-section is divided into a number of fibers and the confined and

unconfined concrete area A_c and A_{c0}, are identified, indicated in red and blue respectively in the cross-section of Figure 1;

d) in order to account for the effect of the strain gradient on the effective FRP lateral confinement acting with different intensity along the depth of the cross-section, the value of confinement pressure for each confined fiber is evaluated as a function of the axial strain through Spoelstra and Monti [25] iterative procedure.

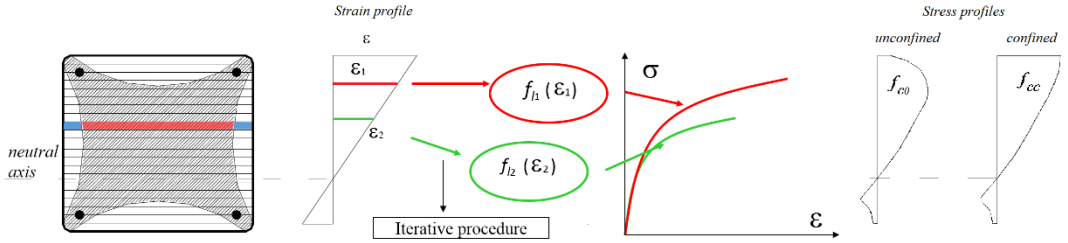

Figure 1 - Fiber model for FRP - wrapped cross-section: starting from a linear strain profile over the cross-section, different FRP-confined concrete laws are obtained for fibers subjected to different longitudinal strain values.

The iterative procedure to evaluate the M-Φ curve for a given cross-section subjected to a constant value of the axial loading $\bar{N}$ is summarized in *Figure 2*. For i-th value of the sectional curvature Φ_i, a trial position of neutral axis x_k is set in order to define the strain profile. Its position will be verified at the end of the cycle by checking the equilibrium condition in longitudinal direction. Constitutive laws for unconfined concrete (Mander's model [36]), for steel bars (Zulfiqar - Filippou model [37]) and concrete in tension (Yankelevsky and Reinhard [38]) are used to obtain the corresponding stress. The complex issue is the evaluation of the compression stress acting at each j-th fiber in the confined area, where the constitutive law is not a-priori defined because it changes with the passive confinement performed by FRP wrapping. The confinement will be larger away from the neutral axis and smaller near it. In the proposed model, in order to capture the variation of the lateral confinement stress $f_{l,j}$ along the depth of the cross-section due to the longitudinal strain gradient, the Spoeltra and Monti iterative model [25] defined for confined concrete under pure axial load is applied here at fiber level.

Once the stress profile is assumed, the compression and tension resultants are easily computed and the axial resultant is evaluated by equilibrium condition in the axial direction. In general, starting from the initial trial value of the neutral axis, the equilibrium condition is searched iteratively. Once the equilibrium is reached, the corresponding moment M is evaluated, obtaining the point of the M-Φ curve. Repeating the procedure for increasing

values of the curvature Φ_i, the entire M-Φ curve for an RC rectangular cross-section under constant axial load $\bar{N}$ can be obtained.

The focus point of the procedure is the evaluation of the distribution of the confinement pressure along the depth of the cross-section. In the present model, each confined fiber is supposed to be part of a circular cross-section with a uniform strain distribution $\varepsilon_{c,ikj}$ (i-th curvature, k-th trial position of the neutral axis, j-th fiber). For each fiber, then, the Spoeltra-Monti procedure is applied setting a trial value of the lateral confinement stress and the iterative procedure is performed until the confinement stress matches the trial value (see *Figure 3*). The iterative procedure is applied for each j-th fiber: starting from its value of longitudinal strain $\varepsilon_{c,ijk}$, the corresponding lateral confinement is iteratively computed and the fiber stress $\sigma_{c,ijk}$ is finally evaluated. It is important to highlight that each fiber has a different confinement level due to the different longitudinal strain. At each curvature step, the Spoeltra-Monti iterative procedure [25] is repeated n times for each k-th trial value of neutral axis position, where n is the number of fibers subject to compression.

In the following, a brief description of the Spoeltra-Monti procedure is reported with its main equations. This procedure, based on Mander's model [36], consider a variable confinement pressure as a function of the axial stress obtained through an iterative procedure summarized in *Figure 3*. In this model, given the longitudinal concrete strain ε_c, the confinement pressure f_l is searched iteratively, starting from a trial value f_{li}. Then, the lateral strain ε_l is obtained adopting the following expression proposed in Pantazopoulou and Mills [39], as a function of the current concrete axial strain and stress, ε_c and σ_c:

$$\varepsilon_l = \frac{E_c \cdot \varepsilon_c - \sigma_c}{2 \cdot \beta \cdot \sigma_c} \tag{1}$$

where E_c is the Young modulus of unconfined concrete, and $\beta = 5700 \Big/ \sqrt{|f_{co}|} - 50$ (N/mm^2) is a concrete property, function of the unconfined concrete strength f_{co}. The longitudinal compressive concrete stress σ_c can be defined following Mander's model [36]:

$$\sigma_c = \frac{f_{cc} \cdot x \cdot r}{r - 1 + x^r} \tag{2}$$

where:

$$x = \frac{\varepsilon_c}{\varepsilon_{cc}} \qquad \varepsilon_{cc} = \varepsilon_{co} \cdot \left[1 + 5 \cdot \left(\frac{f_{cc}}{f_{co}} - 1\right)\right] \qquad r = \frac{E_c}{E_c - E_{\sec}} \qquad E_{\sec} = \frac{f_{cc}}{\varepsilon_{cc}} \tag{3}$$

Moreover, f_{cc} is the maximum confined concrete strength; ε_{cc} is the concrete strain corresponding to f_{cc}; f_{co} is the maximum unconfined concrete strength; ε_{co} is the concrete strain corresponding to è f_{co}; E_{sec} is the secant modulus corresponding to the point (ε_{cc} , f_{cc}).

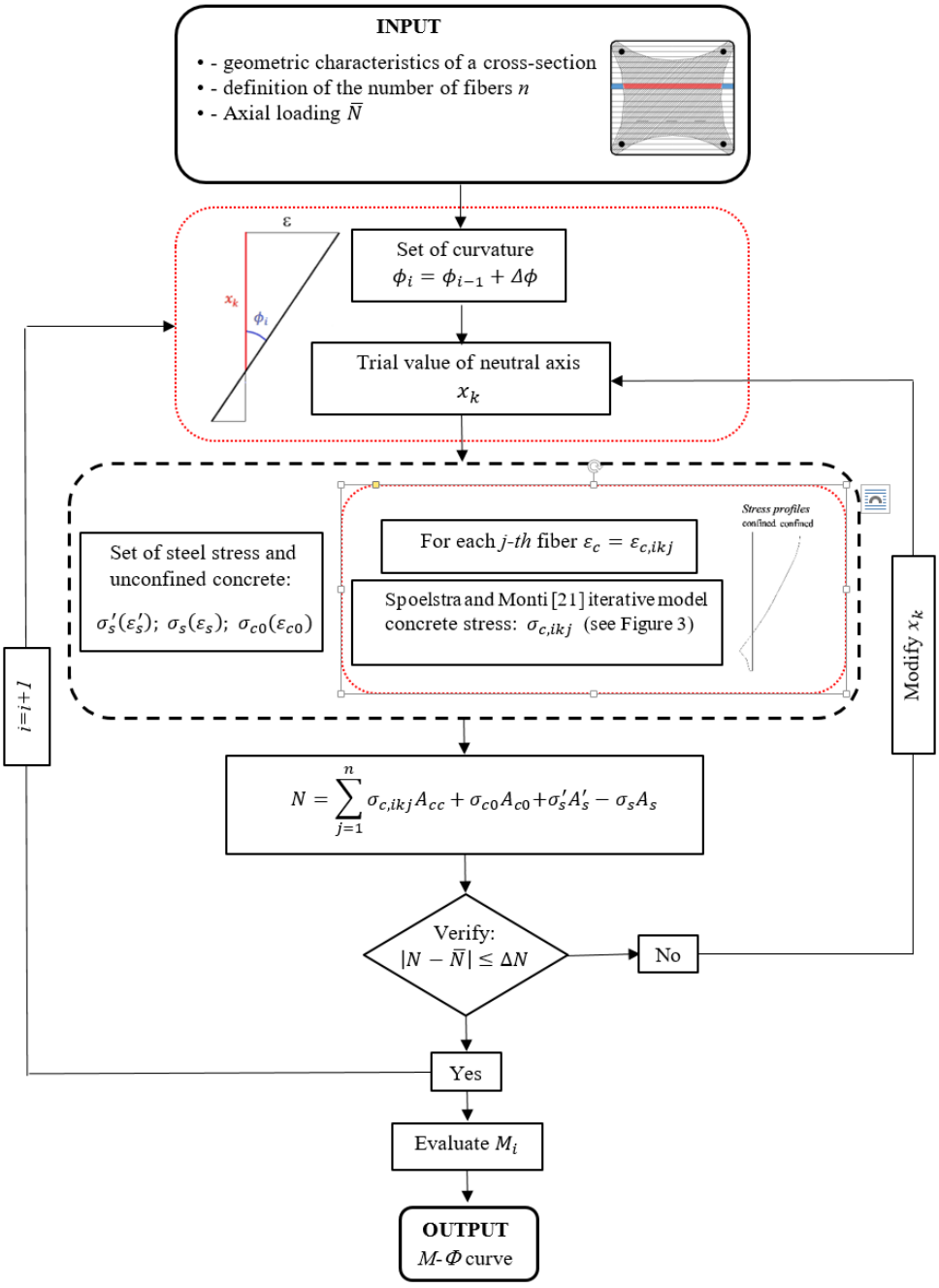

Figure 2 Flowchart of the iterative procedure proposed for the axial-bending analysis of RC cross-section wrapped by FRP.

The maximum confined concrete strength f_{cc} is a function of the lateral confinement pressure f_l due to FRP wrapping, as defined in Mander's model [36]:

$$\frac{f_{cc}}{f_{co}} = 2.354 \cdot \sqrt{1 + 7.94 \cdot \frac{f_l}{f_{co}}} - 2 \cdot \frac{f_l}{f_{co}} - 1.254 \tag{4}$$

The compatibility among axial and lateral strain is described by the equation of Pantazopoulou and Mills [39]:

$$\sigma_c = E_{\text{sec}} \cdot \varepsilon_c \tag{5}$$

$$E_{\text{sec}} = E_c \cdot \frac{1}{1 + 2 \cdot \beta \cdot \varepsilon_l} \tag{6}$$

Then, for an FRP-wrapped cross-section, the confinement pressure f_l can be evaluated through different equations as a function of the lateral strain ε_l of external reinforcement and cross-section shape. For a circular cross-section, f_l can be assessed with the following elastic relation:

$$f_l = \frac{2 \cdot t_j}{d_j} \cdot E_j \cdot \varepsilon_l \tag{7}$$

where t_j, E_j are, respectively, the thickness and the elastic modulus of the composite, and d_j is the cross-section diameter. The confinement pressure f_l is then compared with the trial value, and the iteration goes on up to the condition of confinement pressure matching the tentative value. Employing the Spoelstra and Monti iterative model [25], for a given longitudinal strain ε_l, it is possible to calculate the longitudinal stress accounting for the effective confinement pressure. Moreover, once the lateral strain ε_l is evaluated with eq. (1), the FRP strain ε_j can be assessed and the FRP stress estimated as $\sigma_j = E_j \, \varepsilon_j$. For a circular cross-section, $\varepsilon_j = \varepsilon_l$.

With reference to the hypotheses presented at the beginning of the present section, it can be stated that assumption c), related to the shape effect on the confined area, is correct where the axial strain in concrete is very high, i.e., far from the neutral axis, whereas some error can be introduced, in principle, close to the neutral axis. Nevertheless, close to the neutral axis the concrete is subject to a small strain and, therefore, the difference between confined and unconfined behavior is negligible.

According to assumption d), the confinement pressure is variable over the cross-section, being maximum where compression in concrete is maximum and vanishing at the neutral axis. Of course, in the present model, strain in FRP sheet is then varying along the section contour, e.g., for a rectangular cross-section, it is varying along the two edges orthogonal to the neutral axis. Differently from Binici and Mosalam model [33], the slip in the FRP –

concrete interface is neglected (assumption b). This simplification is motivated by the fact that FRP-concrete interface is very stiff in the linear range [40] and, in practice, no interfacial slip occurs up to the value of external loading close to column failure load. It is also worth remarking that the interfacial shear strength strongly increases when a compression stress state on the interface is present.

The assumption that each confined fiber is supposed to be part of a circular cross-section with a uniform strain distribution $\varepsilon_{c,ikj}$ can introduce some error if the strain gradient in the cross-section is very high (as in the case of high bending with low axial force), but in this case the confinement on the cross-section is less effective, then the error is limited.

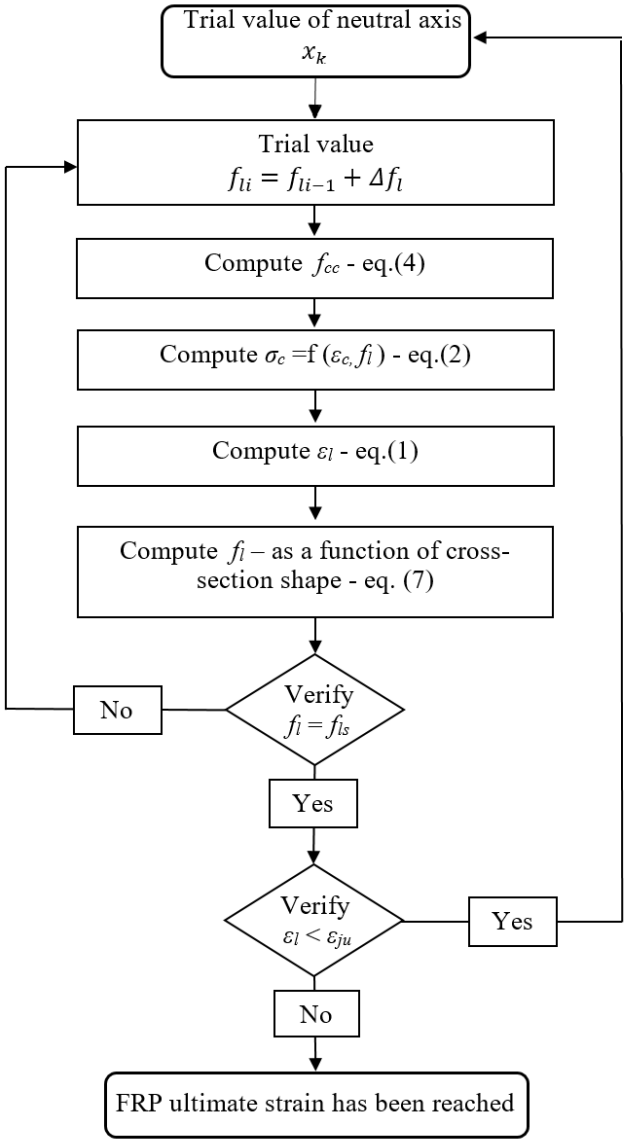

Figure 3 - Iterative procedure for confined concrete proposed by Spoelstra and Monti [25].

2.1 *Confined concrete: unloading curve from compression state*

According to Mander model [36], the value of residual plastic deformation ε_{pl} corresponding to complete unloading ($\sigma = 0$) from a compression state previously reached is defined first (see point C Figure 4). That value is obtained as the value for $\sigma = 0$ of the line joining the initial unloading point $A(\varepsilon_{un}, \sigma_{un})$ with point $B(-\varepsilon_a, -E_c\,\varepsilon_a)$, being E_c the initial elastic modulus and $\varepsilon_a = a\sqrt{\varepsilon_{un}\,\varepsilon_{cc}}$, with $a = \max\left(\varepsilon_{cc}/\varepsilon_{cc} + \varepsilon_{un}, 0.09\,\varepsilon_{un}/\varepsilon_{cc}\right)$ and ε_{cc} the strain corresponding to the maximum strength f_{cc}, i.e.:

$$\varepsilon_{pl} = \varepsilon_{un} - \frac{(\varepsilon_{un} + \varepsilon_a)\,\sigma_{un}}{(\sigma_{un} + E_c\,\varepsilon_a)} \tag{8}$$

For the unloading curve from $A(\varepsilon_{un}, \sigma_{un})$ to $C(\varepsilon_{pl}, 0)$, Mander proposed an expression analogous to that adopted for monotonic loading:

$$\sigma_c = \sigma_{un} - \frac{\sigma_{un} x' r'}{r' - 1 + x'^{\,r'}} \tag{9}$$

where

$$r' = \frac{E_{un}}{(E_{un} - E_c)} \qquad x' = \frac{(\varepsilon_c - \varepsilon_{un})}{(\varepsilon_{pl} - \varepsilon_{un})} \tag{10}$$

and initial unloading modulus is given by $E_{un} = b\,c\,E_c$, with $b = \sigma_{un}/f_{co} \geq 1$, $c = \left(\varepsilon_{cc}/\varepsilon_{un}\right)^{0.5} \leq 1$. It is worth remembering that Mander's theory was originally calibrated for confinement with steel stirrups. Therefore, according to that theory, the unloading curve is defined by neglecting the confinement pressure, since yielding of steel stirrups has been previously reached during loading in compression.

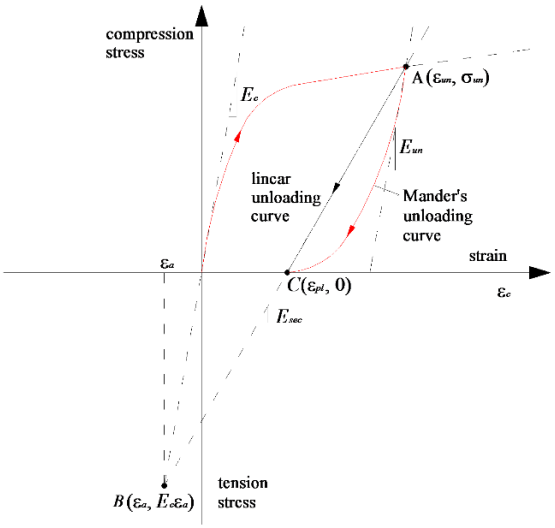

Figure 4 - Loading and unloading branches in compression for confined concrete.

Lam et al. [41] performed some experimental tests of FRP-confined concrete specimens under cyclic compression. In the results presented, the unloading branch has a different shape with respect to the case of non-retrofitted concrete. In fact, due to its linearly elastic behavior, FRP – wrapping exerts a confinement pressure also when concrete is subject to unloading. Hence, the unloading branch tends to be closer to a straight line than in the case of confinement by steel stirrups. Therefore, in the present model for low axial load, the unloading branch has been chosen according to Mander's rule reported in Eq. (9) whereas, for high axial load, the unloading branch is assumed linear between the points A and C of Figure 4. As will be shown in Section 3.2, comparison with experimental results in terms of *M-Φ* curve underlines that, for high values of axial loading, linear unloading curve for confined concrete describes the experimental results better than adopting Mander's unloading curve.

2.2 Concrete under tension

FRP-wrapping has no significant influence on the behavior of concrete under tension. The cyclic behavior of concrete under tension is then modeled starting from Yankelevsky and Reinhardt model [38] (see Figure 5).

Concrete behavior under tension is linear elastic before cracking, occurring when stress reaches the tensile strength $f_{ct} = 0.27(f'_{co})^{2/3}$. The linear elastic branch is modeled through its elastic modulus $E_{\sec} = \sigma_{un}/(\varepsilon_{un} - \varepsilon_{pl})$. According to plasticity theory, for cyclic loading, the origin of the diagram takes the plastic deformation ε_{pl} previously accumulated into account (Figure 5).

The softening branch is then defined by the exponential law:

$$\sigma_c(\varepsilon_c) = f_{ct}\left(1 - \frac{\varepsilon_c - \varepsilon_{ct}}{\varepsilon_{ct}}\right)^2 \qquad (11)$$

where ε_{ct} is the strain corresponding to tensile strength f_{ct}. For strains greater than ε_c= 0.04%, residual strength of concrete under traction vanishes (σ_c=0).

2.3 Reloading curves from tension to compression

Loading curves from tension to compression are modified with respect to Yankelevsky and Reinhardt model [38], even though the general framework is maintained. Reinhardt performed cyclic tests on concrete specimens of small dimensions (50x50x250 mm), applying the tensile loading first up to cracking, then unloading and finally reloading with

compression states. An analytical model was then proposed, with six focus points defining a piecewise linear stiffness of the reloading branch. Reinhardt model requires some modifications in order to be used for full-scale RC columns.

In the present model, two focus points K_1, K_2 are defined along the line with stiffness E_{sec} and origin in the point (ε_{pl}, 0), corresponding to stress levels $k_1 f_{ct}$ and $k_2 f_{ct}$ (see Figure 5). Moreover, k_3 f_{ct} is the tension corresponding to the transition point between the two branches.

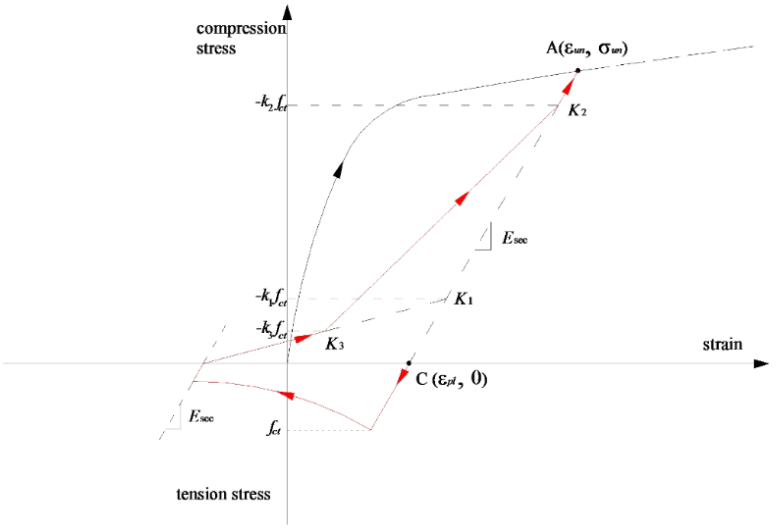

Figure 5 -Tensile behavior of concrete and reloading from tension to compression, with three focus points K_1, K_2, K_3.

The values adopted for parameters k_1, k_2, k_3 are different from those considered in Reinhardt model. In fact, that model was calibrated with reference to experimental results on concrete specimens of small dimensions and without steel reinforcement. Of course, the distance of transverse cracks in concrete has a fundamental role in converting axial elongation measured in experiments to axial deformation to be used in a constitutive model, and concrete cracking in RC columns is very different from that occurred in Reinhardt's small concrete specimens.

In order to calibrate the parameters k_1, k_2, k_3, the cyclic experimental results on circular RC columns without retrofitting under constant axial load and bending moment performed by Abrams [34] were used. According to these calibration studies, the values $k_1 = 1$, $k_2 = 4$, $k_3 = 0.5$ have been adopted in the present model. The comparisons of simulated results and experimental ones are reported in Section 3.

3 VALIDATION OF FRP - CONFINED CROSS SECTIONAL FIBER MODEL

The proposed model has been validated through comparison with some experimental tests available in the literature concerning the cyclic behavior of RC columns subjected to constant axial loading and cyclic bending. In particular, the following experimental tests, whose details are shown in Table 1, have been numerically simulated in Matlab environment:

- unwrapped RC rectangular column tested by Abrams [34], to confirm the model stability without introducing FRP confinement and to calibrate the reloading branch from tension to compression;
- columns with circular cross-section wrapped by FRP jacket tested by Sheikh and Yau [9] where the confinement effect on the whole cross-sectional area is considered;
- columns with square cross-section wrapped by FRP jacket tested by Memon and Sheikh [11], where the cross-section is modeled considering two regions delimitated by parabolas for confined and unconfined concrete, considering the arch effect.

The geometrical dimensions of the cross-sections are the same of the specimens tested (see Table 1). The dimension of fibers adopted to discretize the cross-section is 2 mm, corresponding to a number of fibers equal to 152 and 178, depending on the dimension of the cross-section. The analysis was performed with curvature varying according to the cyclic test procedure and by setting the axial load as a constant value for the entire analysis. The axial load is considered applied in the center of mass of the cross-section.

The main aim of the validation was to verify the reliability of the model to capture the principal parameter such as stiffness, strength, displacement, and hysteretic energy at different cycle amplitudes. It will be shown that in all cases the numerical model predicts well the experimental data in terms of both moment-curvature curves and energy dissipated by hysteretic loops.

Table 1 - Details of test specimens (CFRP: carbon fiber reinforced polymer, GFRP: glass fiber reinforced polymer, ρ_g: geometric steel ratio of longitudinal bars, N: compression axial load, N_u: ultimate load under centered compression, f_y: yield stress of steel bars, f'_{c0}: compressive strength of unconfined concrete).

	Specimens		Longitudinal reinforcement		*N/Nu*	f'_{c0} [MPa]	f_y [MPa]	FRP - No of layers and thickness
	Name	Dimension [mm]	Number and size	ρ_g [%]				

Abrams	-	305 x 230	4 #6 (ϕ = 19.05 mm)	1.6	0.1	42.3	423	-
Sheikh and Yau [9]	ST-2NT CFRP	ϕ = 356 h = 1437	6 M25 (ϕ = 25.2 mm)	3.0	0.54	40.4	450	1 layer 1.25 mm
	ST-3NT GFRP	ϕ = 356 h = 1437	6 M25 (ϕ = 25.2 mm)	3.0	0.56	40.4	450	1 layer 1.00 mm
	ST-4NT CFRP	ϕ = 356 h = 1437	6 M25 (ϕ = 25.2 mm)	3.0	0.27	44.8	450	1 layer 0.5 mm
	ST-5NT GFRP	ϕ = 356 h = 1437	6 M25 (ϕ = 25.2 mm)	3.0	0.27	40.4	450	1 layer 1.25 mm
Memon and Sheikh	ASG-3NSS GFRP	305 x 305 h = 1473	8 M20 (ϕ = 19.5 mm)	2.58	0.56	42.7	465	2 layers 1.25 mm
	ASG-4NSS GFRP	305 x 305 h = 1473	8 M20 (ϕ = 19.5 mm)	2.58	0.56	43.3	465	4 layers 1.25 mm
	ASG-6NSS GFRP	305 x 305 h = 1473	8 M20 (ϕ = 19.5 mm)	2.58	0.56	44.2	465	6 layers 1.25 mm

3.1 Simulation of Abrams [34] *tests on unwrapped columns*

In order to calibrate the reloading branch from tension to compression for concrete, Abrams tests were used, leading to the calibration parameters k_1, k_2, k_3 subsequently adopted in all the other simulations.

In Figure 6, the experimental results by Abrams [34] and numerical simulations are compared in terms of moment-rotation curve. The rotation is obtained by multiplying the curvature by the length of displacement transducer (254 mm). The specimens were subjected to a constant axial loading of 300 kN, corresponding to about 10% of the ultimate axial loading N_u. The results are in good agreement in terms of both yielding moment (about 110 kN m) and unloading and reloading branches for increasing values of maximum rotation. The cycle shapes in the second and fourth quadrant, i.e., where stress in concrete changes its sign from tension to compression and vice-versa, are very well reproduced. In particular, the reloading branches from tension to compression were used to calibrate the parameters $k_1 = 1$, $k_2 = 4$, $k_3 = 0.5$. The so calibrated parameters k_1, k_2, k_3 defining the reloading branches of the cyclic constitutive law of concrete were then used in all the following simulations.

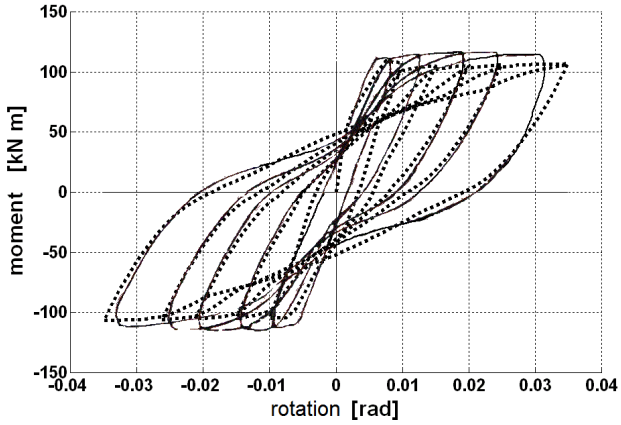

Figure 6 - Moment – rotation diagram for unwrapped RC column cross-section under constant axial force and cyclic bending. Experimental results from [34] *(—) and numerical results (- - -).*

3.2 *Simulation of Sheikh and Yau* [9] *tests on circular columns*

The first comparison for the validation of the proposed model was carried out for circular columns tested under a constant axial loading and cyclic bending by Sheikh and Yau [9]. The diameter of the cross-section is 356 mm. The details of FRP reinforcements are summarized in Table 2, in terms of type of material (CFRP and GFRP), thickness, elastic modulus E, ultimate stress f_{ju} and ultimate strain ε_{ju}.

Table 2 – Sheikh and Yau [9] *tests, details of FRP reinforcements.*

FRP	Thickness (mm)	E (MPa)	f_u (MPa)	ε_u (%)
CFRP	0.5	150000	1800	1.2
CFRP	1	75000	900	1.2
GFRP	1.25	20000	400	2

The comparison with experimental tests by Sheikh and Yau [9] is shown in Figure 7*a,c* for low axial force (N/N_u=0.27, N_u being the ultimate load under centered compression) and Figure 7*b,d* for high axial force (N/N_u=0.54). For reloading of concrete from tension to compression, the same values of parameters k_1, k_2, k_3 calibrated from Abrams test [34] were adopted here.

Even though the experimental results exhibit an unsymmetrical behavior when moment changes its sign (no equal values of yielding moments for positive and negative bending), unloading and reloading branches are very well predicted. Modeling of these branches is fundamental in order to obtain a realistic value of the dissipated energy of hysteretic loops. The comparison clearly shows that the pinching effect is well predicted because the contribution of concrete in tension in the reloading branch is taken into account, as shown

in Figure 7, with a consequent optimal evaluation of the dissipated energy by hysteretic loops. In the numerical curves, the failure points are reported adopting as the failure criterion the achievement of the 60% of FRP ultimate strain as will be discussed in Section 4.

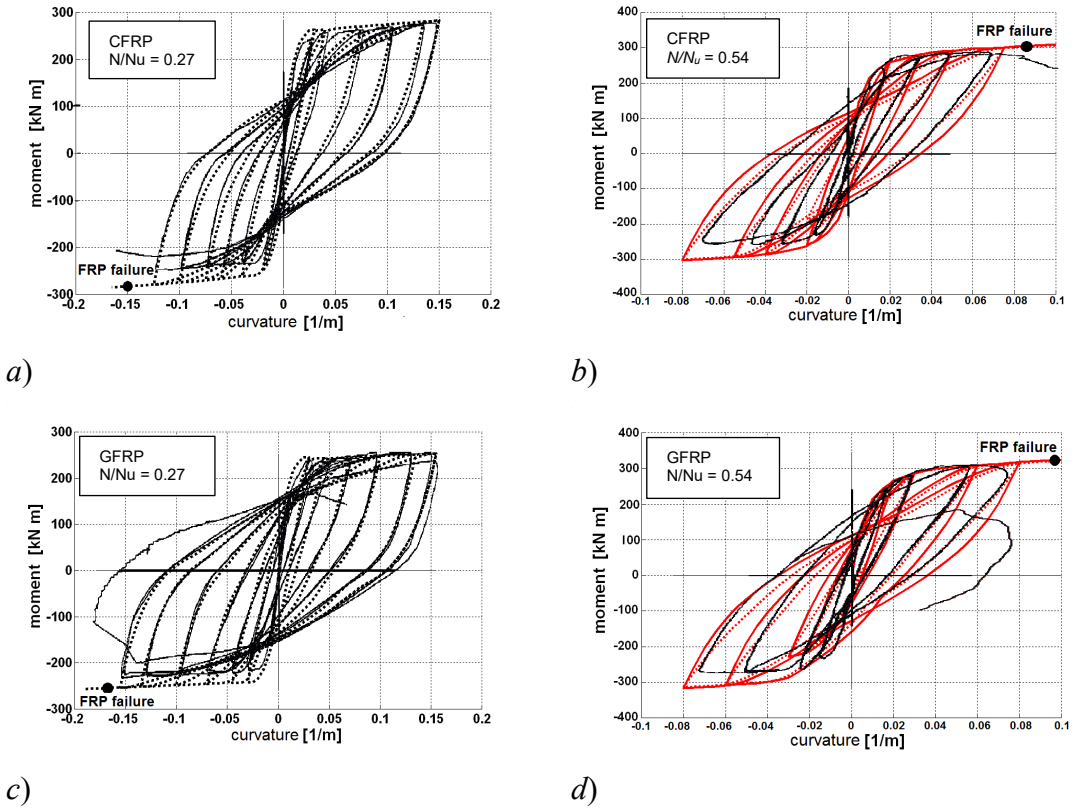

Figure 7 - Moment – curvature diagrams for FRP – wrapped circular RC column cross-sections under constant axial force and cyclic bending: experimental results (—) from Sheikh and Yau [9]*; numerical results adopting Mander's unloading curve (- - -) and adopting linear unloading curve (—); Specimens* a*) ST-4NT, b) ST-2NT,* c*) ST-5NT,* d*) ST-3NT.*

Finally, in Figure 7*b,d,* where tests at high values of axial force are simulated, two different numerical curves are reported: dashed line refers to unloading according to Mander's model, whereas solid line refers to the modified rule proposed in this study (elastic unloading, see Section 3.2.4). The comparison shows that unloading curves are very well reproduced for high axial force if elastic unloading is adopted. On the contrary, for low axial force, good agreement is found adopting Mander's unloading curve. For this reason, only the curve obtained using Mander's unloading branch is reported in Figure 7*a,c* and compared with experimental data.

The final investigation concerns the hysteretic loops for cyclic bending with constant axial force. With reference to tests by Sheikh and Yau [9], the comparison between values of hysteretic damping factors ς at different levels of maximum curvature μ_c obtained by post-

processing experimental data and from numerical simulations are depicted in Figure 6*a,b* (low axial load) and Figure 6*c,d* (high axial load). Both predictions adopting Mander's and linear unloading curve (see Section 2.2) are reported. For low axial loads, the criterion adopted to define the unloading curve (Mander's curve or elastic unloading) has a small influence on the damping factor. For high axial loads, the influence of the confinement is much more significant and elastic unloading gives a better prediction of damping factor. Finally, note that the damping factor is smaller when elastic unloading is adopted. Mander's unloading curve then gives non-conservative results on dissipated energy by hysteresis loops for high values of axial force.

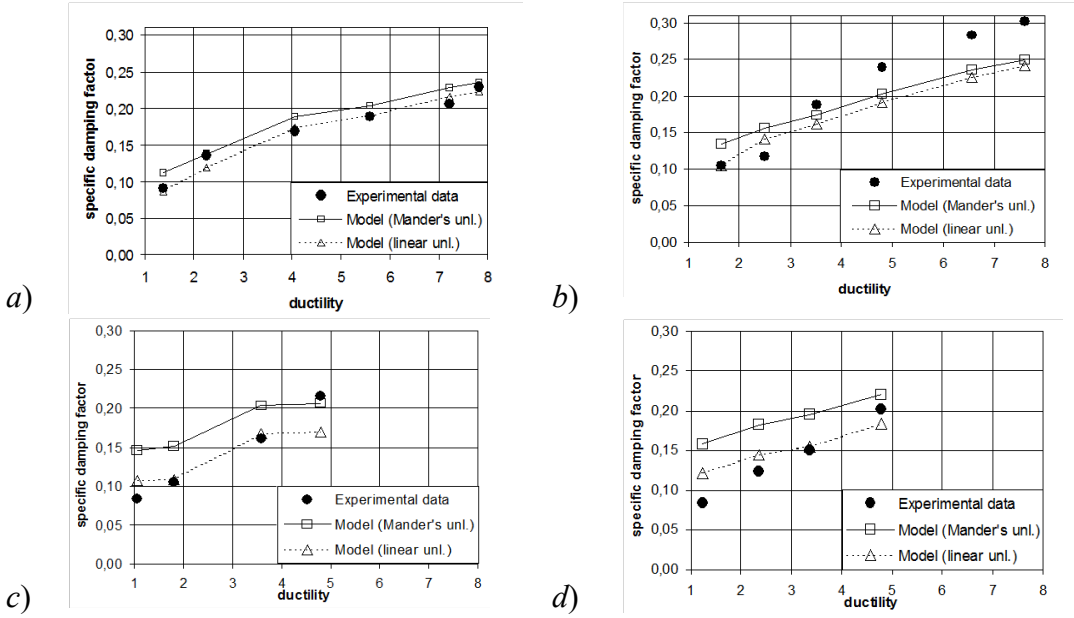

Figure 8 - Specific damping ratio vs cycles at different levels of ductility: specimens a) *ST-4NT,* b) *ST-5NT, (*N/N_u *= 0.27);* c) *ST-2NT,* d) *ST-3NT (*N/N_u *= 0.54).*

3.3 Simulation of Memon and Sheikh [11] *tests on square columns*

Finally, the comparison with experimental tests by Memon & Sheikh [11] on the cyclic behavior of columns with square cross-section strengthened by glass (GFRP) composites are shown in Figure 9. The GFRP wrapping system has a thickness of 1.25 mm. The average properties of the composite materials are ultimate strength f_u = 563 MPa, ultimate strain ε_u 2.28 %, and the elastic modulus E = 24693 MPa.

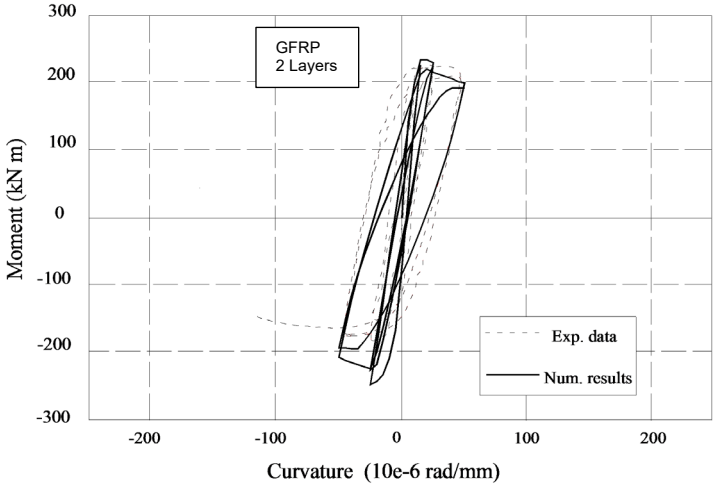

a)

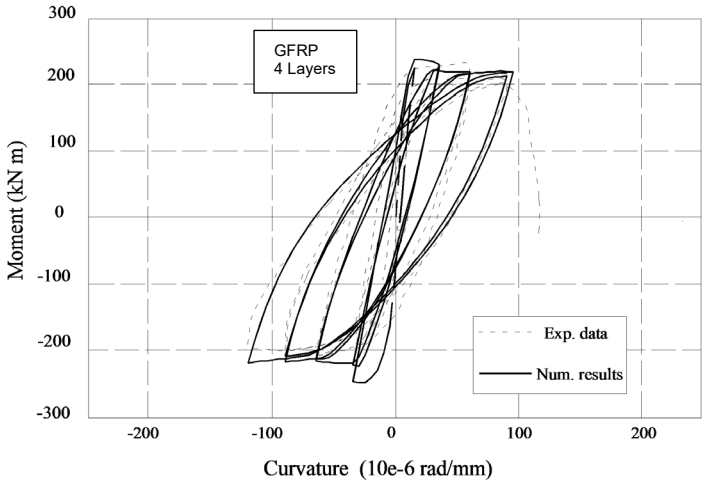

b)

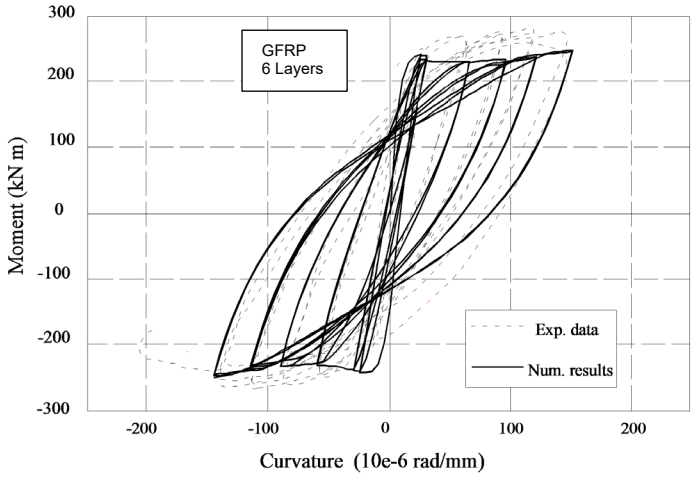

c)

Figure 9 - Moment – curvature diagrams for FRP – wrapped square RC column cross-sections under constant axial force and cyclic bending. Experimental results from Ref. [11] *and numerical results with the proposed model: specimens* a*) ASG-4NSS (2 GFRP),* b*) ASG-3NSS (4 GFRP),* c*) ASG-6NSS (6 GFRP).*

In numerical simulations, the unloading branch is assumed linearly elastic due to the high value of axial force, and confined and unconfined areas of the concrete cross-section are defined according to [35]. First of all, the results clearly show the beneficial effect of wrapping. By comparing results for increasing numbers of layers of GFRP (Figure 9*a*,*b*,*c*), it can be verified that the curvature before the onset of column strength degradation increases significantly. Moreover, the comparison between experimental and numerical results shows that the proposed model is able to correctly predict yield moment and, in almost all cases, also the shape of hysteretic loops at different values of maximum curvature.

4 PUSHOVER ANALYSES FOR RC FRAMES WITH COLUMNS WRAPPED BY FRP

A push-over analysis for a non-ductile RC frame retrofitted by FRP-column wrapping was performed implementing the proposed iterative constitutive model in OpenSees [42] software, using a Finite Element with distributed plasticity. A new *Uniaxial Material* was implemented, named *Concrete_conf.cpp,* accounting for the entire iterative procedure with loading and reloading branches described in Section 2. The required parameters are unconfined concrete strength f_{co} and relative strain ε_{co}, FRP ultimate strain $\varepsilon_{j,rup}$, FRP Young modulus E_j, and geometrical percentage of FRP over the cross-section $\rho_j=4t_j/D$ (circular cross-section) or $\rho_j=4t_j/B$ (rectangular cross-section, B being the smallest dimension of the cross-section).

A portal frame and a 4-floor frame structure are considered. The static non-linear analysis was selected rather than the dynamic one in order to better understand the global behavior of the non-ductile RC frame and its structural deficiencies, and for estimating the effectiveness of different retrofitting strategies. However, the implemented model can be applied also to carry out non-linear dynamic analyses thanks to the implemented cyclic constitutive law.

The pushover analysis was performed with force distributions proportional to the first modal shape by adopting a displacement-based procedure.

The formulation based on flexibility matrix and forces is used for nonlinear finite elements for beams and columns. Five control sections are adopted to describe the nonlinear behavior of materials along the element by adopting a fiber discretization of the cross-section and enforcing plane strain assumption. The spread of plasticity along the element is directly taken into account by the fiber model. The use of finite elements with distributed plasticity

is particularly important in the case of FRP-confinement columns because the definition of the plastic hinge length in the case of FRP-wrapping is still an open issue.

4.1 Structural failure criteria

In order to estimate the capacity of the structure by means of the pushover analysis, the ultimate condition must be adequately defined. To this aim, two main approaches, based respectively on the definition of ultimate strain or ultimate chord rotation, can be followed. According to the first criterion, the ultimate condition is reached when, in some points of the structure, an ultimate value of strain is attained. In particular, for the unretrofitted structure, the ultimate condition corresponds to the attainment of the ultimate strain of concrete while, for the retrofitted structure, the attainment of 60 percent of the ultimate strain of FRP, corresponding to the rupture of FRP – wrapping according to Teng et al. [17], is considered. For an unretrofitted RC frame, this approach could be considered too local and too conservative, because the damaged element can be able to distribute/transfer the stress to other members, and a local failure criterion could not allow determining the ultimate condition at the building level. Contrarily, for FRP wrapped column the attainment of the ultimate strain (composite rupture) involves the failure of the reinforcement strategy, so it can be considered a realistic failure criterion for the structural element, and then for the entire structure. The adopted failure criterion is the attainment of the ultimate strain of FRP reduced by 40 percent (see Ref. [17]).

With reference to the second criterion, the increment of rotational capacity for an FRP-wrapped RC column with respect of the unwrapped one was shown by Biskinis and Fardis [43], that collected an extended database with more than 200 tests with the aim of calibrating a formulation for the ultimate chord rotation of FRP-wrapped RC columns starting from mechanical and geometrical cross-section parameters, including FRP ultimate strain.

In the following numerical example, both the described criteria were adopted and compared for evaluating the structural ultimate capacity. In particular, for the first criterion, corresponding to the attainment of jacket deformation equal to 60 percent of its ultimate deformation [17], the FRP strain is here calculated and checked at each iteration according to equations 5-7.

4.2 *Single bay frame*

As a first example, a single-bay single-floor frame is considered. The geometric characteristics and mechanical properties for steel reinforcement, unconfined concrete, and FRP–wrapping are given in Figure 10 and Table 3, respectively.

The portal frame is subject to a distributed load q = 30 kN/m and to two vertical forces, N, applied to the columns to simulate the presence of upper floors. Four different values of N are considered, N = 0, 180 kN, 360 kN, 540 kN.

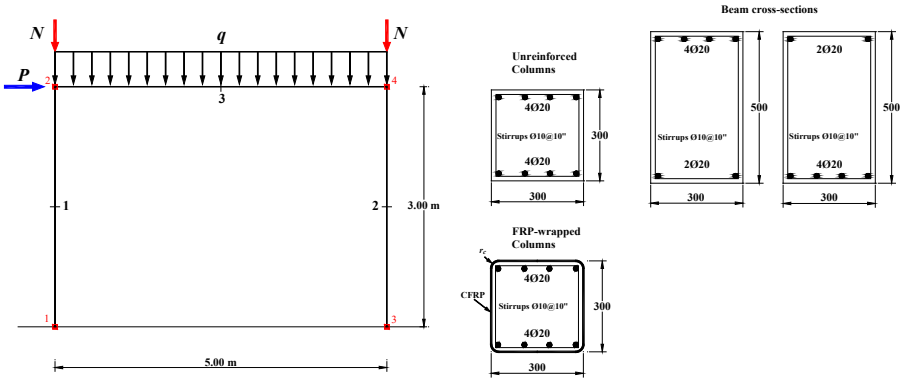

Figure 10 – Single-bay frame structure: geometry and cross-sections of beam and columns (unwrapped and FRP-wrapped case).

Table 3 - Mechanical properties of materials considered for the single-bay frame.

Steel bars	f_y = 414 MPa	E_0 = 210000 MPa	b = 0.009
Unconfined concrete	f'_{c0}= 30 MPa	ε_{co} = 0.0022	ε_{cu} = 0.0035
FRP - wrapping	t = 1 mm	E_{FRP} = 231000 MPa	$\varepsilon_{j,\,rup}$ = 0.0072

In Figure 11, the results of pushover analysis are reported in terms of base shear – top displacement curves, considering both cases, i.e. columns unreinforced and reinforced by FRP – wrapping. No second-order effects are considered in the analyses. The ultimate displacements are shown, corresponding to different failure criteria: attainment of ultimate strain in a column or ultimate chord rotation for unwrapped and wrapped RC members. The ultimate chord rotation is computed according to Eurocode 8 [44] for unwrapped columns and by Biskinis and Fardis formulation [43] for wrapped columns.

The presence of FRP –wrapping leads to significant benefits, strongly increasing the ductility of columns, with consequent larger displacements attained. In particular, in the unwrapped frame, when the ultimate strain ε_{cu} in column base sections is attained, a remarkable ductility reduction occurs, with increasing N, whereas concrete confinement by

wrapping allows reaching very large displacements. Moreover, it is possible to note that, for the unwrapped case, the two different failure criteria (ultimate strain or ultimate chord rotation) lead to similar estimates of the ultimate top displacement. On the contrary, the differences are significant for the reinforced case, where failure due to the attainment of ultimate strain always precedes the one based on the ultimate chord rotation estimated by Biskinis and Fardis [43]. Hence, the ultimate strain failure criterion corresponding to FRP rupture, after which the confinement action instantaneously drops to zero, is more conservative with respect to the ultimate chord rotation. For this reason, ultimate strain deformation is adopted as the failure criterion for the following example.

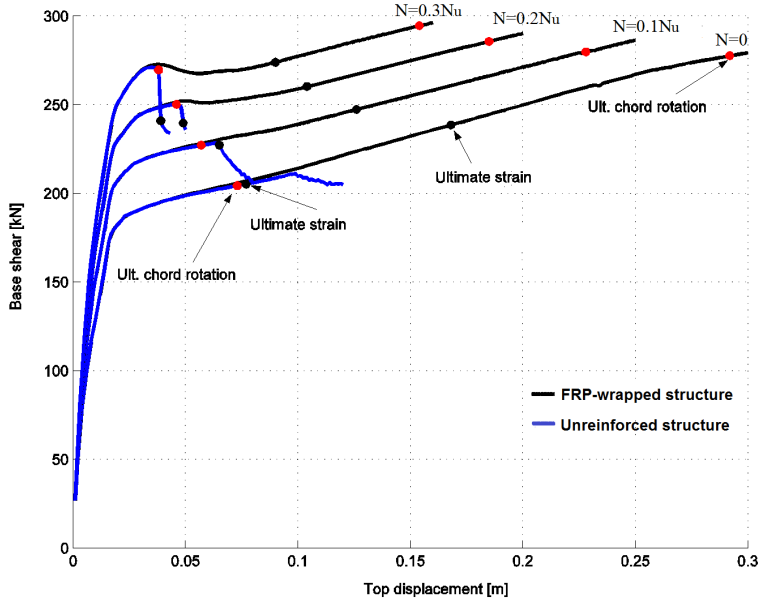

Figure 11 - Pushover analysis of a single-bay frame subject to different values of axial load on columns. Unwrapped structure and structure with reinforced columns by FRP-wrapping. Comparison between ultimate displacements computed through different failure criteria.

4.3 Pre-code RC Building

In this section, a 4-floor RC frame structure showing a soft floor behavior is studied. Geometrical and mechanical properties are reported in

Figure 12 and Table 4. It is worth noting that, between the second and the third floor, the columns present a reduction of the cross-section and of the amount of longitudinal steel, as frequently observed in pre-code buildings. The beams are subject to a distributed vertical load q = 20 kN/m.

The frame structure performances in the pre-intervention condition highlight a soft story mechanism on the third floor due to the change in column stiffness and observed by

analyzing the interstory drift. In order to improve the building seismic response, two types of FRP reinforcement strategies are proposed: a global wrapping reinforcement to all columns with 2 FRP layers or, alternatively, two local wrapping reinforcements of columns of the third floor with a different number of FRP layers, respectively equal to 3 and 6 layers.

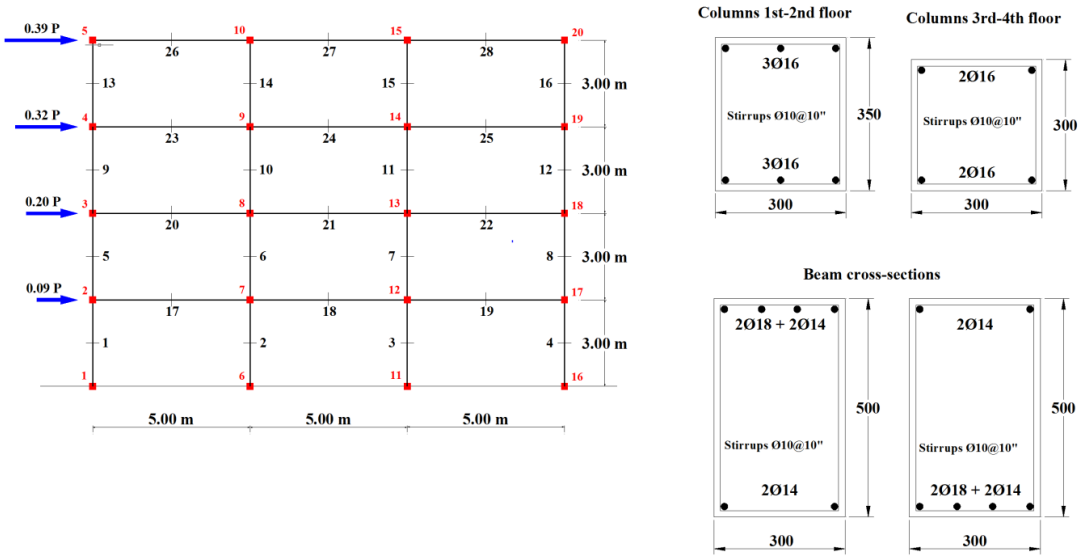

Figure 12 - 4-floor frame structure: geometry and cross-sections of beam and columns (unwrapped and FRP-wrapped columns).

Table 4 - Mechanical properties of materials adopted for the 4-floor frame.

Steel bars	f_y = 414 MPa	E_0 = 414 MPa	b = 0.009
Unwrapped concrete	f'_{c0} = 30 MPa	ε_{cu} = 0.0022	ε_{cu} = 0.0035
FRP - wrapping	t_1= 0.165 mm/layer	E_{FRP} = 231000 MPa	$\varepsilon_{j,rup}$ = 0.0072

The results of pushover analysis in terms of capacity curves are shown in Figure 13, considering the unwrapped structure and the three different strengthening strategies for the reinforced structure. It is possible to note that, with all strengthening methods, the stiffness of the structures is almost unmodified, but the displacement capacity of the structure is significantly increased, with the third solution (wrapping of the columns of the 3rd floor with 6 layers) being the best solution.

The evolution of interstory drift and horizontal floor displacements at different values of top displacement up to the ultimate condition are reported in Figure 14 for two cases: the unwrapped structure (Figure 14*a*); the strengthened structure with a local reinforcement with 6 layers of FRP (Figure 14*b*). Figure 14*a* confirms that the failure of the unwrapped frame is due to a soft floor mechanism occurring at the third-floor level. By the local

strengthening reinforcement, the displacement capacity is significantly increased as shown in Figure 14b.

In order to evaluate the different effects of the adopted strategies, the interstory drift and horizontal floor displacement at the ultimate condition for unwrapped structure, global reinforced with 2 layers, and local reinforced with 6 layers are compared in Figure 15. The local solution (wrapping of the columns of the 3rd floor with 6 layers) significantly increases the displacement capacity as can be seen in Figure 14 and Figure 15.

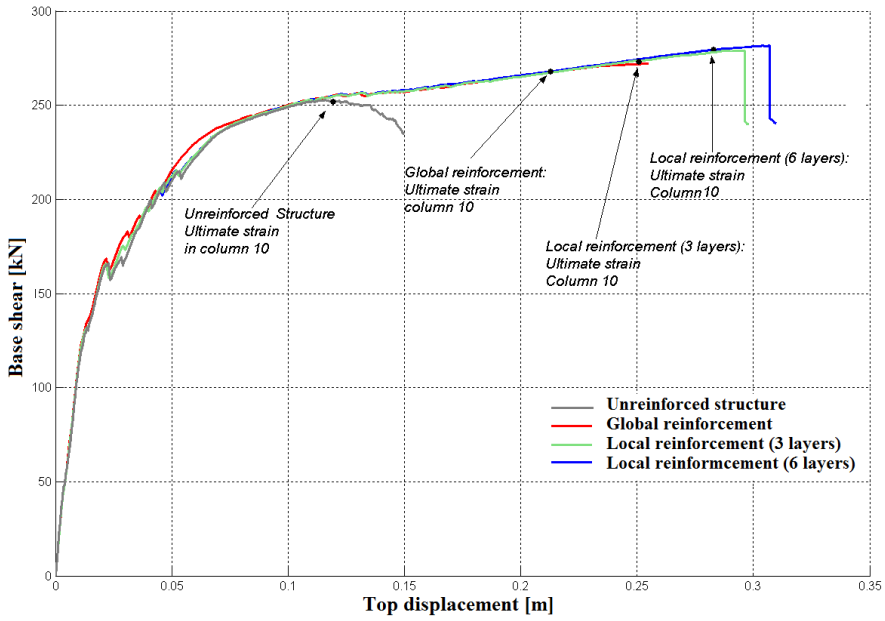

Figure 13 - Pushover analysis on a 4-floor RC frame: unwrapped structure and retrofitted structure with FRP-column wrapping adopting 3 different strengthening strategies.

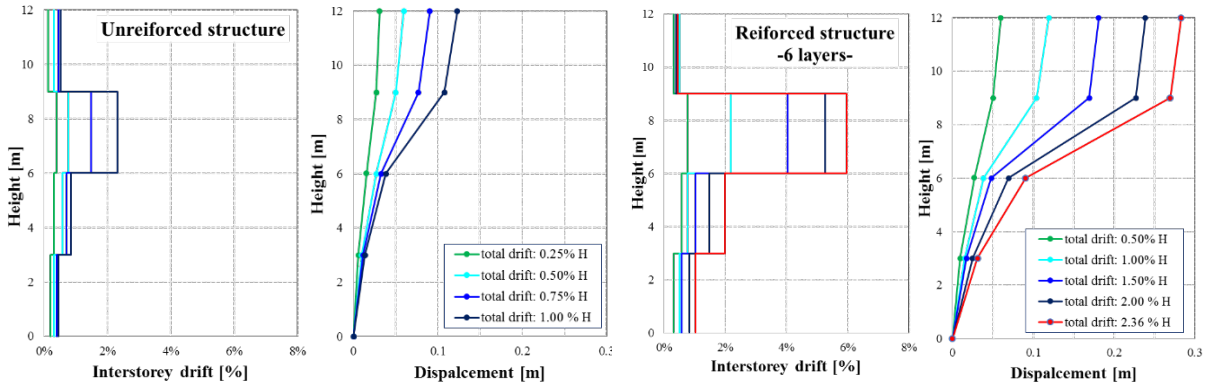

a) *b*)

Figure 14 - Pushover analysis of a 4-floor RC frame. Interstory drift and horizontal displacements at different total drift up to failure: a) unwrapped structure and b) retrofitted structure with 6 CFRP layers for columns of the 3rd floor.

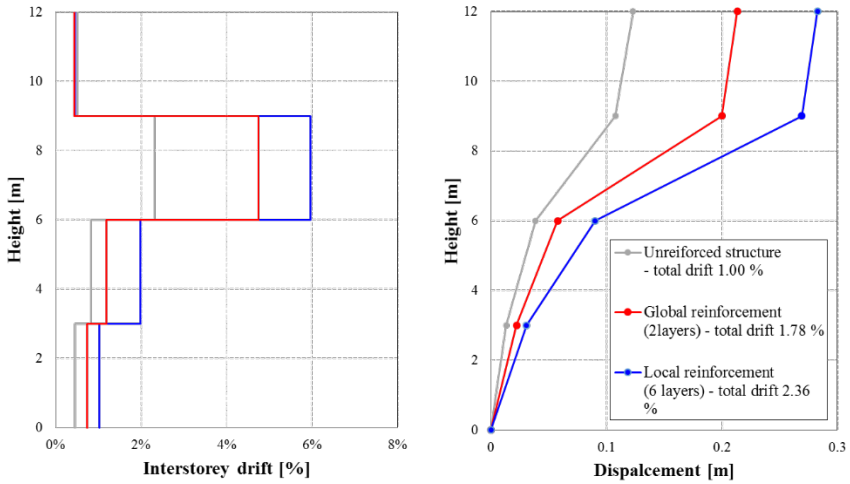

Figure 15 - Pushover analysis of a 4-floor RC frame. Interstory drift and horizontal displacements at the ultimate condition for unwrapped structure, global reinforcement with 2 layers, and local reinforcement with 6 CFRP layers at the 3rd floor.

The final failure mechanism predicts the formation of plastic hinges with a top displacement of about 2.5 times greater than in the unwrapped case. Values of displacement at yielding and ultimate displacement for the unwrapped case and the strengthened frames are shown in Table 5.

It is worth noting, as a final comment on the outputs of the case study, that being the soft story at the third floor, no significant second-order effects were expected. Of course, in the case of soft-story mechanism at a lower floor, a strengthening technique based on column ductility increase can lead to large displacements that can be unacceptable for a frame structure. Hence, in most cases, FRP-wrapping of columns must be associated with other strategies that limit the deformability of the structures.

Table 5 - Unreinforced and FRP – wrapped RC frames; displacement at yielding δ_1, ultimate displacement δ_u, structural ductility ratio δ_u/δ_1 and total drift (top displacement divided by as the height of the structure H=*12 m).*

	δ_1(m)	δ_u (m)	δ_u/δ_1	*Total Drift*
Unreinforced frame	0.045	0.1195	2.66	1% *H*
2 layers CFRP wrapping (global reinforced)	0.045	0.213	4.73	1.78% *H*
3 layers CFRP wrapping (3rd floor only)	0.045	0.251	5.58	2.09% *H*
6 layers CFRP wrapping (3rd floor only)	0.046	0.283	6.15	2.36% *H*

5 CONCLUSIONS

The present work is focused on the behavior of RC columns wrapped by Fiber Reinforced Polymer sheets, subjected to axial force and cyclic bending. A cross-sectional model for rectangular cross-sections, implemented in Matlab environment, is developed. The main strengths of the present model are: i) the shape effect of the cross-section on confinement is accounted by the arch effect; ii) the confinement pressure is considered not constant during the loading steps guaranteeing the compatibility of longitudinal and transversal deformation; iii) at each step the confinement pressure is variable over the cross-section and consequently each concrete fiber has a specific constitutive law depending on the effective lateral pressure; iv) unloading and loading branches are properly defined in order to correctly predict the pinching effects and, consequently, the energy dissipation by hysteresis.

The reliability of the proposed iterative cyclic cross-sectional model has been assessed by comparison with some experimental results reported in the literature, for different reinforcement types and values of the axial load. Results obtained from numerical simulations are in very good agreement with experimental test results of unwrapped and FRP wrapped RC columns, considering both circular and square cross-sections. Furthermore, the hysteretic damping coefficient has been evaluated as a function of maximum attained curvature and, also in this case, good agreement between experimental and numerical data is shown.

Subsequently, the proposed model has been implemented in a finite element software with distributed plasticity, OpenSees package, for performing structural non-linear analysis of RC frames built without seismic requirements and retrofitted by FRP-column wrapping.

A pushover analysis has been performed considering a portal frame and a 4-floor RC frame structure, for which capacity curves and interstory drifts are calculated. The failure mechanism of the unreinforced structures has been estimated, giving useful information to choose the most appropriate strategy of retrofitting. The 4-floor unreinforced RC frame exhibited a soft-floor mechanism, and wrapping of RC columns by FRP sheet has been chosen in order to increase ductility. Two types of reinforcement strategies have been examined: reinforcing columns of the soft floor only or wrapping all columns of the structure. The first choice, with 6 layers of carbon FRP, has been showed to be not only the less invasive but also the more effective in terms of structure ductility, about 2.5 times greater than for the unretrofitted structure.

The selected case study puts in evidence the importance to evaluate the non-linear behavior of existing structures reinforced with different interventions in order to select the most efficient for the specific case. With this purpose, the proposed model is able to capture the effectiveness of FRP-wrapping in terms of increment of strength and, mainly, of ductility and can be effectively implemented in FE models to perform nonlinear analyses of frame structures.

6 ACKNOWLEDGEMENTS

The authors wish to acknowledge the financial support received by the Italian Department of Civil Protection (ReLUIS 2019-2021 Grant).

7 REFERENCES

[1] P. Ricci, F. de Luca, G.M. Verderame, 6th April 2009 L'Aquila earthquake, Italy: Reinforced concrete building performance, Bull. Earthq. Eng. 9 (2011) 285–305. doi:10.1007/s10518-010-9204-8.

[2] R. Ferlito, M. Guarascio, M. Zucconi, Assessment of a vulnerability model against post-earthquake damage data: The case study of the historic city centre of L'Aquila in Italy, in: 9th World Conf. Earthq. Resist. Eng. Struct. A Coruna, Spain, 8-10 July, WIT Transactions on the Built Environment, 2013: pp. 393–404. doi:10.2495/ERES130321.

[3] J.G. Ruiz-Pinilla, J.M. Adam, R. Pérez-Cárcel, J. Yuste, J.J. Moragues, Learning from RC building structures damaged by the earthquake in Lorca, Spain, in 2011, Eng. Fail. Anal. 68 (2016) 76–86. doi:10.1016/j.engfailanal.2016.05.013.

[4] M. Del Zoppo, M. Di Ludovico, A. Balsamo, A. Prota, G. Manfredi, FRP for seismic strengthening of shear controlled RC columns: experience from earthquakes and experimental analysis, Compos. Part B Eng. 129 (2017) 47–57. doi:10.1016/j.compositesb.2017.07.028.

[5] C.M. Ramirez, A.B. Liel, J. Mitrani-Reiser, C.B. Haselton, A.D. Spear, J. Steiner, G.G. Deierlein, E. Miranda, Expected earthquake damage and repair costs in reinforced concrete frame buildings, Earthq. Eng. Struct. Dyn. 41 (2012) 1455–1475. doi:10.1002/eqe.

[6] F. Romano, M. Faggella, R. Gigliotti, M. Zucconi, B. Ferracuti, Comparative seismic

loss analysis of an existing infilled RC building based on element fragility functions proposals, Eng. Struct. 177 (2018) 707–723. doi:10.1016/j.engstruct.2018.08.005.

[7] F. Romano, M.S. Alam, M. Faggella, M. Zucconi, A.R. Barbosa, B. Ferracuti, Seismic loss analysis of a modern RC building accounting for uncertainty of infill strut modeling parameters, in: M. Papadrakakis, M. Fragiadakis (Eds.), COMPDYN 2019 -7th ECCOMAS Themat. Conf. Comput. Methods Struct. Dyn. Earthq. Eng., 2019: pp. 24–26.

[8] A. Balsamo, A. Colombo, G. Manfredi, P. Negro, A. Prota, Seismic behavior of a full-scale RC frame repaired using CFRP laminates, Eng. Struct. 27 (2005) 769–780. doi:10.1016/j.engstruct.2005.01.002.

[9] S.A. Sheikh, G. Yau, Seismic behavior of concrete columns confined with steel and fiber-reinforced polymers, ACI Struct. J. 99 (2002) 72–80. doi:10.14359/11037.

[10] G. Lignola, A. Prota, G. Manfredi, E. Cosenza, Experimental performance of RC hollow columns confined with CFRP, J. Compos. Constr. 11 (2007) 72–80. doi:10.1061/(ASCE)1090-0268(2007)11:1(42).

[11] M.S. Memon, S.A. Sheikh, Seismic resistance of square concrete columns retrofitted with glass fiber-reinforced polymer, ACI Struct. J. 102 (2005) 774–783. doi:10.14359/14673.

[12] O. Ozcan, B. Binici, G. Ozcebe, Seismic strengthening of rectangular reinforced concrete columns using fiber reinforced polymers, Eng. Struct. 32 (2010) 964–973. doi:10.1016/j.engstruct.2009.12.021.

[13] R. Realfonzo, A. Napoli, Results from cyclic tests on high aspect ratio RC columns strengthened with FRP systems, Constr. Build. Mater. 37 (2012) 606–620. doi:10.1016/j.conbuildmat.2012.07.065.

[14] H.F. Ghatte, M. Comert, C. Demir, A. Ilki, Evaluation of FRP confinement models for substandard rectangular RC columns based on full-scale reversed cyclic lateral loading tests in strong and weak directions, Polymers (Basel). 8 (2016). doi:10.3390/polym8090323.

[15] H.F. Ghatte, M. Comert, C. Demir, A. Ilki, Seismic performance of full-Scale FRP Retrofitted substandard RC columns loaded in the weak direction, 847 (2016) 347–353. doi:10.4028/www.scientific.net/AMM.847.347.

[16] A. Pavese, D. Bolognini, S. Peloso, FRP seismic retrofit of rc square hollow section bridge piers, J. Earthq. Eng. 8 (2004) 225–250. doi:10.1080/13632460409350526.

[17] J.G. Teng, J.F. Chen, S.T. Smith, L. Lam, FRP: strengthened RC structures, Front.

Phys. (2002) 266. doi:10.1002/pi.1312.

[18] M.N. Youssef, M.Q. Feng, A.S. Mosallam, Stress-strain model for concrete confined by FRP composites, Compos. Part B Eng. 38 (2007) 614–628. doi:10.1016/j.compositesb.2006.07.020.

[19] M.F.M. Fahmy, Z. Wu, Evaluating and proposing models of circular concrete columns confined with different FRP composites, Compos. Part B Eng. 41 (2010) 199–213. doi:10.1016/j.compositesb.2009.12.001.

[20] L. Lam, J.G. Teng, Design-oriented stress–strain model for FRP-confined concrete, Constr. Build. Mater. 17 (2003) 471–489. doi:10.1016/S0950-0618(03)00045-X.

[21] M. Samaan, A. Mirmiran, M. Shahawy, Model of concrete confined by fiber composites, J. Struct. Eng. 124 (1998) 1025–1031. doi:10.1061/(ASCE)0733-9445(1998)124:9(1025).

[22] N.F. Hany, E.G. Hantouche, A.M. Asce, M.H. Harajli, Axial stress-strain model of CFRP-confined concrete under monotonic and cyclic loading, J. Compos. Constr. 19 (2015) 1–16. doi:10.1061/(ASCE)CC.1943-5614.0000557.

[23] A. Ilki, O. Peker, E. Karamuk, C. Demir, N. Kumbasar, FRP retrofit of low and medium strength circular and rectangular reinforced concrete columns, J. Mater. Civ. Eng. 20 (2008) 169–188. doi:10.1061/(ASCE)0899-1561(2008)20:2(169).

[24] A. Mirmiran, M. Shahawy, A new concrete-filled hollow FRP composite column, Compos. Parte B Eng. 8368 (1996) 263–268. doi:1359-8368(95)00019-4.

[25] M. Spoelstra, G. Monti, FRP-confined concrete model, J. Compos. Constr. 3 (1999) 143–150. doi:10.1061/(ASCE)1090-0268(1999)3:3(143).

[26] A. Fam, S. Rizkalla, Confinement model for axially loaded concrete confined by circular fiber-reinforced polymer tubes, ACI Struct. J. (2001) 451 –61.

[27] B. Binici, An analytical model for stress-strain behavior of confined concrete, Eng. Struct. 27 (2005) 1040–1051. doi:10.1016/j.engstruct.2005.03.002.

[28] J.G. Teng, Y.L. Huang, L. Lam, L.P. Ye, Theoretical Model for Fiber-Reinforced Polymer-Confined Concrete, J. Compos. Constr. (2007) 201–211. doi:10.1061/(ASCE)1090-0268(2007)11:2(201)CE.

[29] J.C. Lim, T. Ozbakkaloglu, Unified stress-strain model for FRP and actively confined normal-strength and high-strength concrete, J. Compos. Constr. 19 (2015). doi:10.1061/(ASCE)CC.1943-5614.0000536.

[30] O. Chaallal, M. Shahawy, Performance of fiber-reinforced polymer-wrapped reinforced concrete column under combined axial-flexural loading, ACI Struct. J. 97

(2000) 659–668. doi:10.14359/7433.

[31] J.G. Teng, L. Lam, G. Lin, J.Y. Lu, Q.G. Xiao, Numerical simulation of FRP-jacketed RC columns subjected to cyclic and seismic loading, J. Compos. Constr. 20 (2016) 04015021. doi:10.1061/(ASCE)CC.1943-5614.0000584.

[32] A.M. Ismail, M.F.M. Fahmy, Z. Wu, Simulating the lateral performance of FRP-confined RC circular columns using a new eccentric-based stress-strain model, Compos. Struct. 180 (2017) 88–104. doi:10.1016/j.compstruct.2017.07.075.

[33] B. Binici, K.M. Mosalam, Analysis of reinforced concrete columns retrofitted with fiber reinforced polymer lamina, Compos. Part B Eng. 38 (2007) 265–276. doi:10.1016/j.compositesb.2006.01.006.

[34] D.P. Abrams, Influence of axial force variation on flexural behaviour of reinforced concrete columns, ACI Struct. J. 84. (1987) 246–254.

[35] A. Mirmiran, M. Shahawy, M. Samaan, H. El Echary, J.C. Mastrapa, O. Pico, Effect of column parameters on FRP-confined concrete, J. Compos. Constr. 2 (1998) 175–185. doi:10.1061/(ASCE)1090-0268(1998)2.

[36] J.B. Mander, M.J.N. Priestley, R. Park, Theoretical Stress-Strain Model for Confined Concrete, J. Struct. Eng. 114 (1988) 1804–1826. doi:10.1061/(ASCE)0733-9445(1988)114:8(1804).

[37] F. Filippou, N. Zulfiqar, Models of critical regions in reinforced concrete frames under earthquake excitations, Earthq. Eng. Res. Cent. Tech. Rep. 90-06. (1990).

[38] D. Yankelevsky, H.W. Reinhardt, Uniaxial behavior of concrete in cyclic tension, J. Struct. Eng. 115 (1989) 166–182. doi:10.1061/(ASCE)0733-9445(1989)115:1(166).

[39] S. Pantazopoulou, R. Mills, Microstructural aspects of the mechanical response of plain concrete, ACI Mater. J. 92-M62 (1996) 605–616.

[40] B. Ferracuti, M. Savoia, C. Mazzotti, Interface law for FRP-concrete delamination, Compos. Struct. 80 (2007) 523–531. doi:10.1016/j.compstruct.2006.07.001.

[41] L. Lam, J.G. Teng, C.H. Cheung, Y. Xiao, FRP-confined concrete under axial cyclic compression, Cem. Concr. Compos. 28 (2006) 949–958. doi:10.1016/j.cemconcomp.2006.07.007.

[42] Pacific Earthquake Engineering Research Center, OpenSees – Open System for earthquake engineering simulation, (n.d.).

[43] D. Biskinis, M.N. Fardis, Models for FRP-wrapped rectangular RC columns with continuous or lap-spliced bars under cyclic lateral loading, Eng. Struct. 57 (2013) 199–212. doi:10.1016/j.engstruct.2013.09.021.

[44] EC8-3, Eurocode 8: Design of structures for earthquake resistance - Part 3: Assessment and retrofitting of buildings, 2005.